# CAS3D: An Intuitive Software Package to Apply 3D Structural Analysis on 3D Multiphoton Microscopy Data of Skeletal Muscle Single Fibers

Dominik Schneidereit*,1, Chloë Gossens[2], Oliver Friedrich[1]

***Abstract*— Keep the abstract to 250 words or less.**

***Index Terms*— Enter about five key words or phrases in alphabetical order, separated by commas.**

## I. Introduction

MULTIPHOTON microscopy allows for the non-invasive, label-free detection of the 3-Dimensional molecular arrangement of the actin-myosin lattice within muscle cells and fibres using Second Harmonic Generation (SGH) signal [1], [2]. The technique offers access to large volumes of high-resolution data of the cellular morphology in 3D [3], [4]. Manual evaluation of the data to extract significant descriptors is possible but tedious on 2D slices of the 3D voxel matrix. Several tools are available to speed up this kind of 2D or slice-wise semi 3D analysis process [5], [6] or post-process 3D images [7]. As of now, however, there are no comprehensive tools available to perform a 3D analysis on this kind of voxel data which is close to impossible to perform manually. We designed, implemented and tested a software package that extracts morphometric parameters from 3D voxel arrays of artificial test data and real image data of mouse single fibres. The software design is focused lowering the entry threshold to using the software by offering an intuitive GUI, automatic processing of multiple data sets and folder trees, automatic generation of output graphs and offering an all-in-one software installer package. The software was applied in differentiating between septic and healthy EDL muscle in different treatment groups of mice via the resulting morphometric characteristics [8].

## II. Methods

### A. Sample preparation

24 week old male 57BL/6JRj Mice (Janvier SAS, CHassal, France) of a sepsis treatment model of the Department of Cellular and Molecular Medicine were used as tissue donors [8], [9]. The Institutional Ethical Committee for Animal Experimentation of the KU Leuven approved the protocols for the animal studies (internal project numbers P124/2017 and P062/2019). The *extensor digitorum longus* (EDL) muscles were extracted and fixed in phosphate buffered saline with 3% para-formaldehyde solution. They were transferred to the imaging facility where single muscle fibers were manually mechanically isolated.

### B. Microscopy

Label-free multiphoton imaging of the myosin structure of mechanically isolated myofibres was performed on an upright TrimScope II, similar to the previously published system [10]. The excitation was performed with an Nikon ??? objective and a average laser power of 150 mW carrying an average pulse energy of 1.9 nJ. An U-AAC condenser lens (OLYMPUS, Japan) was applied to collect transmitted light. The second harmonic generation (SHG) signal was filtered with a band pass filter 20 nm bandwith and a center wavelnength of 405 nm (Chroma Technology, Germany). Autofluorescence was collected via the ??? excitation objective and filtered with a bandpass filter with 50 nm bandwith and a center wavelength of 525 nm (Chroma Technology, Germany). Intensity signals were recorded with non-descanned photomultiplier tubes (H 7422-40 LV 5 M, Hamamatsu Photonics, Japan). Image stacks of myofibres were acquired with a voxel size of 0.2 µm × 0.2 µm × 0.5 µm and a field of view of 100 µm × 100 µm with a stack depth of typically 50 µm.

### C. Software functionality ???

Myofibrillar parallelism was determined by the cosine angle sum (CAS) parameter, as described before [11] with adjustments. The dominant sarcomere direction vector $\vec{m}$ and local voxel direction vectors $\vec{v}_i$ were determined in 3D, meaning that the angle $\phi$ of each local voxel vector was located in the common plane of $\vec{v}_i$ and mvector, and not in the XY-cardinal plane. As illustrated in Fig. 1 A 3D fast Fourier transform was performed on the image stacks to obtain $\vec{m}$ from particle analysis in the 3D Fourier space; 9×9×9 voxel 3D Sobel kernels were convolved with the image stack to obtain the three-component local voxel direction vector $\vec{v}$ for each voxel

Submission date 15.12.2022 Sponsors and financial acknowledgment
* Corresponding author dominik.schneidereit@fau.de
[1] Insitute of Medical Biotechnology, Friedrich-Alexander Universität Erlangen-Nürnberg
[2] Clinical Division and Laboratory of Intensive Care Medicine, Department of Cellular and Molecular Medicine, KU Leuven, Leuven, Belgium

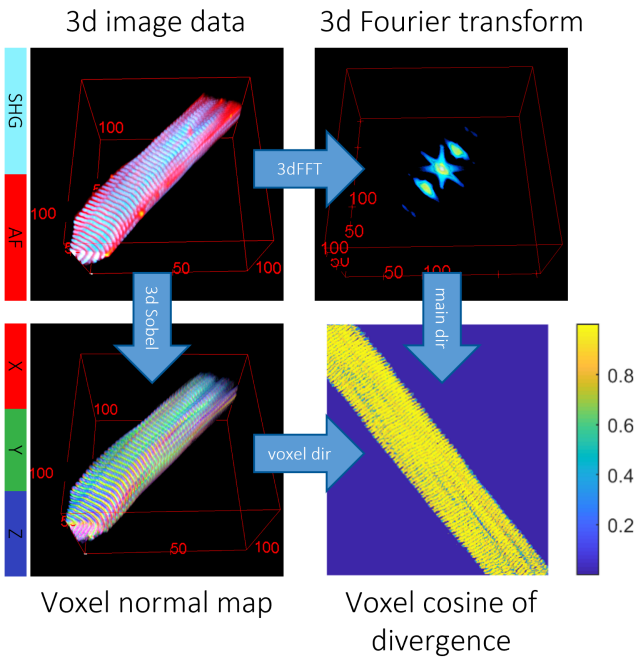


Fig. 1. **A visual representation of the major image processing steps that were performed on a 3D image of a mouse muscle fibre. (A)** a 3D reconstruction of the multi-channel raw data showing SHG signal in Teal and Autofluorescence signal in Red. The channel containing SHG signal is separated from the data set and exclusively used in the analysis process. **(B)** A 3D-Fourier space representation of the SHG voxel data in false colors. A particle analysis on the Fourier space data is used to determine the dominant orientation and frequency of the repeating sarcomere lattice pattern of the sample. **(C)** A false color 3D reconstruction of the normal vector representation of the SHG voxel data. Each voxel is color coded for the orientation of its normal vector with the cardinal vector components in X, Y and Z-direction are represented in Red, Green and Blue. The vector magnitude is represented with voxel intensity. **(D)** A central slice image of the voxel data that describe the cosine of the angular divergence between dominant orientation of the sarcomeric lattice pattern and the normal orientation vector of each voxel. Voxels with normal vectors in alignment with the dominant pattern alignment yield values close to 1, dis-alignment reduces the value to a minimum of 0 at perfect perpendicularity to the dominant alignment pattern.

i. The determination of CAS was performed using MATLAB (MATLAB R2018b, The MathWorks Inc., USA).

## III. Results

### A. Software results presentation and significant numbers

### B. Evaluation of ideal datasets

Several ideal data objects (Fig. 4) were created in Fiji. All objects were made from 512x512x512 voxels with 32bit floating point intensity values in each voxel. The intensity data was normalized between 1.0 and 0.0. The objects were supplemented with meta data that define the SL of repeating patterns to be 2µm. The Gaussian sphere object serves as a non-patterned isotropic sample. It was generated with its maximum at the center voxel of the volume and a spherical falloff with a standard deviation of 64 voxels. The object yields a CAS3d of 0.5 as is expected of a isotropic object. Even though the object features no visible repetitive pattern, a pattern length of 0.3µm was determined. This is an effect of

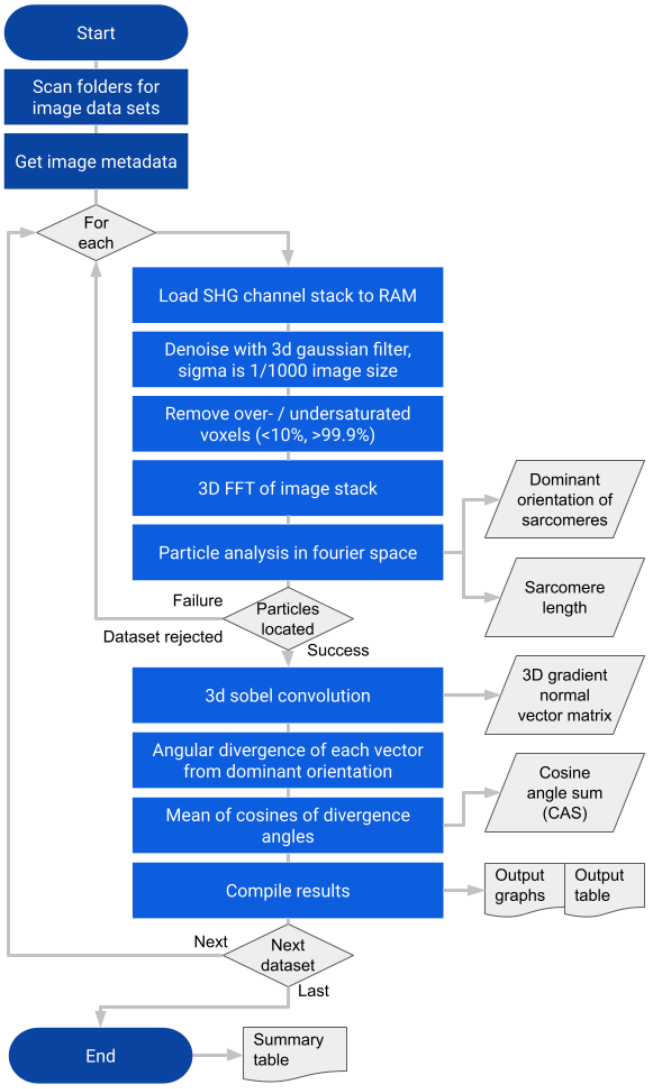


Fig. 2. **An ISO 5807 standard flowchart of the CAS3D software function.** The major functionalities and generated outputs are summarized. Processes are shown in Blue rectangles, decision forks are represented as Gray diamonds. The resulting data from specific process steps is shown in Gray parallelograms, generated output files are indicated as rectangles with a wavy bottom edge.

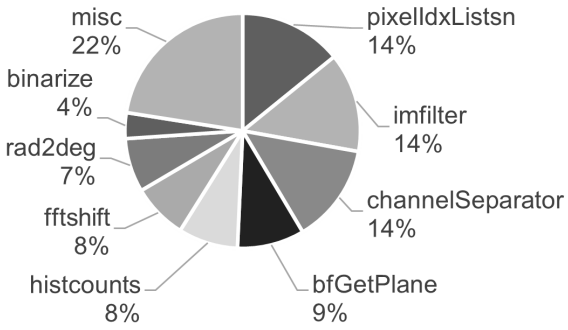


Fig. 3. **Software run-time fractions spent in specific functions.**

low-level noise that was detectable in Fourier space and likely is a product of the cubic shape of the voxels (see appendix 1

for further detail on the noise). ??? Maybe background removal artifact??? A sphere wave pattern is used as a isotropic but regularly patterned test object, as such it yields a CAS3d of 0.5 and the set SL of 2µm is detected. A Sine wave pattern is used as ideal oriented and structured object. Its detected CAS3d is 1.0 and the set SL is 2µm. A sine wave cylinder pattern is used to approximate an idealized muscle fiber. The test object yields a CAS3d close to 1.0. The CAS3d in the sine wave cylinder is slightly lower than that of a perfect sine wave pattern due to the gradients at the edges of the cylinder that are aligned perpendicular to the dominant pattern orientation.

Sine wave patterns of different orientation were supplemented with increasing amounts of random noise in order to assess the precision of the detection of the orientation and pattern size parameters (Fig. 5). The standard deviation of the added random noise intensity is provided as a percentage of the maximum image intensity.

A sample set of sine wave pattern objects with 2µm SL as well as both orientation and elevation values of 0°, 20°, 40°, 60° and 80° is each supplemented with 1% 5%, 10% and 20% random noise, creating a sample set of 55 voxel objects with well defined initial parameters. The mean deviation of the detected SL from the specified value is +0.004µm (0.2%) with a standard deviation of the detection of ±0.006µm (0.3%). While the deviation is small, it can not be disregarded according to a zero hypothesis t-test (P<<0.001). The pattern orientation is detected with a mean deviation of -0.006° from the set orientation with a standard deviation of ±0.05°. The pattern elevation is detected with a mean deviation from the set elevation of -0.004° with a standard deviation of ±0.05°. The deviations in both orientation and elevation detection are statistically indistinguishable from zero according to a zero hypothesis t-test (P¿0.1).

No significant correlation (Pearson P >> 0.05) between applied random noise and the error in other determined parameters (SL, orientation, elevation) within the testing range (0-20% random noise) could be detected. Ori and elev deviation outlier with 0.3° at 10% random noise and 80° in both cases, weird because random noise was added seperately, only the ideal grid was flipped from ori to elev axis

Correlation of CAS to random noise: Pearson correlation test yields very strong correlation (P << 0.05) with positive sign, predicting a dropping CAS with increase in random noise amount in data of a perfect pattern. The correlation appears to be linear (see fig) with a slope of -0.006 ±2.5x$10^{-5}$ (StdDev). When a random noise with a standard deviation of 82% of the signal intensity is added on top of a ideal signal pattern, it is no longer distinguishable from an isotropic signal by the software.

When noise intensity is further increased, the reduction in CAS lessens. The correlation can be well described with a Boltzmann-correlation, as the original pattern never gets replaced but is supplemented with random noise.

### C. Evaluation of mouse single fibre datasets

## IV. Conclusion

## Supplemental Files

## Acknowledgment

## References

[1] S. Schürmann, C. Weber, R. H. A. Fink, and M. Vogel, "Myosin rods are a source of second harmonic generation signals in skeletal muscle," p. 64421U.

[2] S. V. Plotnikov, A. C. Millard, P. J. Campagnola, and W. A. Mohler, "Characterization of the Myosin-Based Source for Second-Harmonic Generation from Muscle Sarcomeres," vol. 90, no. 2, pp. 693–703.

[3] S. Plotnikov, V. Juneja, A. B. Isaacson, W. A. Mohler, and P. J. Campagnola, "Optical Clearing for Improved Contrast in Second Harmonic Generation Imaging of Skeletal Muscle," vol. 90, no. 1, pp. 328–339.

[4] L. Mercier, J. Böhm, N. Fekonja, G. Allio, Y. Lutz, M. Koch, J. G. Goetz, and J. Laporte, "In vivo imaging of skeletal muscle in mice highlights muscle defects in a model of myotubular myopathy," vol. 5, no. 1, p. e1168553.

[5] A. Buttgereit, C. Weber, and O. Friedrich, "A novel quantitative morphometry approach to assess regeneration in dystrophic skeletal muscle," vol. 24, no. 7, pp. 596–603.

[6] D. Schneidereit, "Second Harmonic Generation Morphometry of Muscle Cytoarchitecture in Living Cells," in *Cell Viability Assays: Methods and Protocols 2nd Edition* (D. F. Gilbert and O. Friedrich, eds.), Methods in Molecular Biology, Springer.

[7] C. Lefort, M. Chalvidal, A. Parenté, V. Blanquet, H. Massias, L. Magnol, and E. Chouzenoux, "FAMOUS: A fast instrumental and computational pipeline for multiphoton microscopy applied to 3D imaging of muscle ultrastructure," vol. 54, no. 27, p. 274005.

[8] C. Goossens, R. Weckx, S. Derde, L. V. Helleputte, D. Schneidereit, M. Haug, B. Reischl, O. Friedrich, L. V. D. Bosch, G. V. den Berghe, and L. Langouche, "Impact of prolonged sepsis on neural and muscular components of muscle contractions in a mouse model," vol. 12, no. 2, pp. 443–455.

[9] S. Derde, S. Thiessen, C. Goossens, T. Dufour, G. Van den Berghe, and L. Langouche, "Use of a Central Venous Line for Fluids, Drugs and Nutrient Administration in a Mouse Model of Critical Illness," no. 123, p. 55553.

[10] D. Schneidereit, S. Nübler, G. Prölß, B. Reischl, S. Schürmann, O. J. Müller, and O. Friedrich, "Optical prediction of single muscle fiber force production using a combined biomechatronics and second harmonic generation imaging approach," vol. 7, no. 1, p. 79.

[11] A. Buttgereit, C. Weber, C. S. Garbe, and O. Friedrich, "From chaos to split-ups - SHG microscopy reveals a specific remodelling mechanism in ageing dystrophic muscle: Remodelling of dystrophic muscle," vol. 229, no. 3, pp. 477–485.

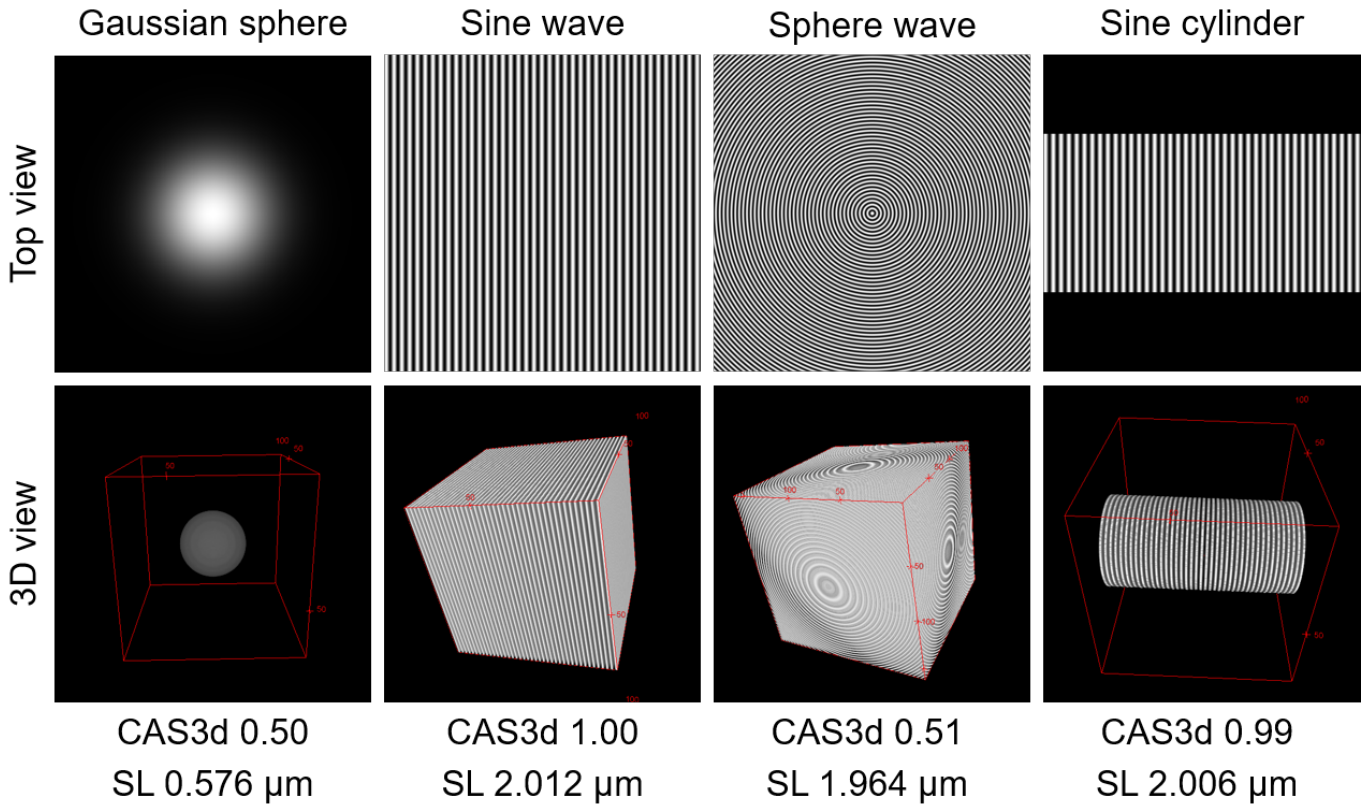


Fig. 4. **A gallary of the artificial voxel objects used for software validation.** A half cut view through the center and a stereoscopic view is shown of each voxel object. A spherical Gaussian gradient was used as a unpatterned isotropic sample with a gradient. It yields the expected CAS3d value of 0.5. The regular sine wave pattern with a spacing (SL) of 2µm is used to validate orientation, SL and CAS3d detection (see Fig. 5) and yields the expected CAS3d of 1.0. A spherical wave patten is used to simulate a patterned but isotropic sample, yielding the expected CAS3d of 0.5 with a good reproduction of the mean pattern spacing of 2µm . A cylindrical sine wave pattern is used as a idealized representation of a muscle fibre. Even though the the pattern within the cylinder is ideal, the CAS3d slightly deviates from a 1.0 due to the gradients at the edges of the cylinder that is perpendicular to the dominant pattern orientation.

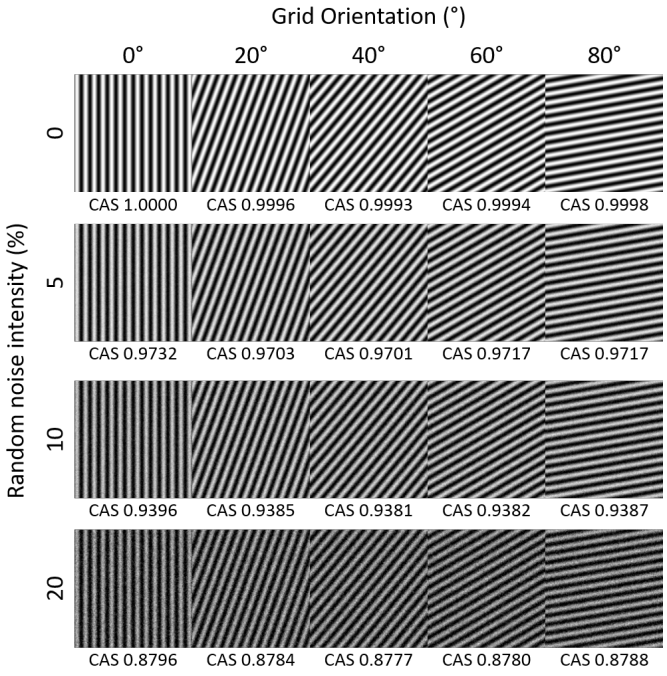


Fig. 5. **CAS3d of sine wave grids and its correlation to orientation and random noise magnitude.** The gallery shows the top down view on half cut views of the sine wave voxel objects. All objects consist of 512x512x512 32bit floating point voxels with intensities between 0.0 and 1.0 . The object pattern is oriented between 0°-80°. The objects are supplemented with random noise with a standard deviation of 0%-20% of the maximum image intensity. The CAS3d varies slightly with the dominant orientation and is inversely correlated to applied random noise (see Fig. 7 for details).

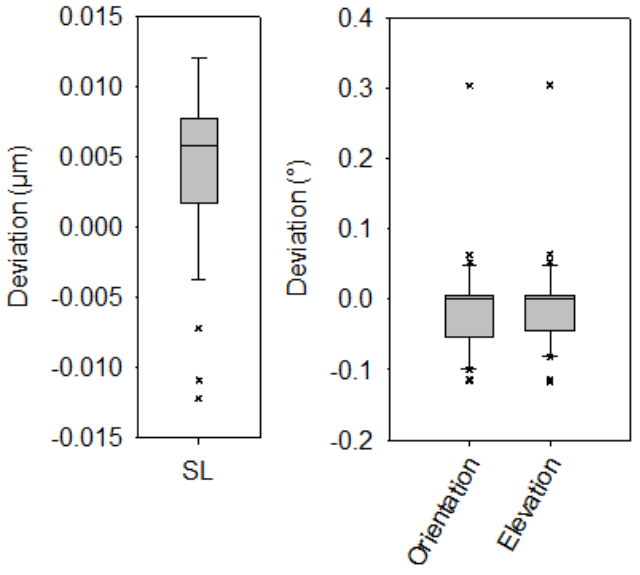


Fig. 6. **Deviation of detected pattern length (SL) and orientation from the set values in sine wave grids.** The predefined SL of 2 µm is on average detected too large by 4 nm across all noise intensities and orientations with a standard deviation of 6 nm. On average, the pattern orientation is detected too low by 0.005° with a standard deviation of 0.05° for all random noise intensities. Similarly, the elevation is on average detected too low for 0.004° with a standard deviation of 0.05°. ## add zero hypothesis test results!##

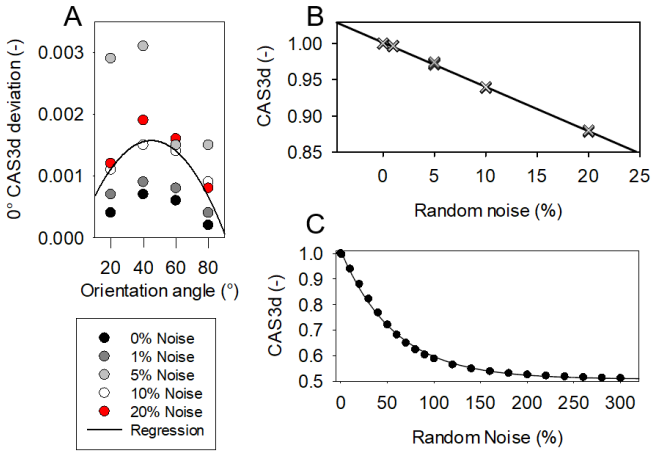


Fig. 7. **The effects of sample orientation and random noise on CAS3d detection. A:** The deviation of CAS3d values of sine pattern objects of different orientation compared to respecive 0° oriented objects with the same noise intensity. A Gaussian regression fit is used to visualize the deviation trend. The deviations of CAS3d tend to increase to an average maximum of 0.0015 at 45° orientation. There seems to be no direct correlation between random noise intensity and the CAS3d deviation, as the highest deviation values around 0.003 appear at 5% random noise intensity. **B:** The random noise intensity has a inverse correlation to the CAS3d (Pearson P << 0.05). The correlation appears to be linear in the noise intensity range from 0% to 20% with a slope of -0.006 (CAS3d / % noise). **C:** When the noise intensity is increased up to 300% the correlation between CAS3d and noise intensity can be best described with a Boltzmann function, as the initial pattern gets gradually overwhelmed by the added random noise.

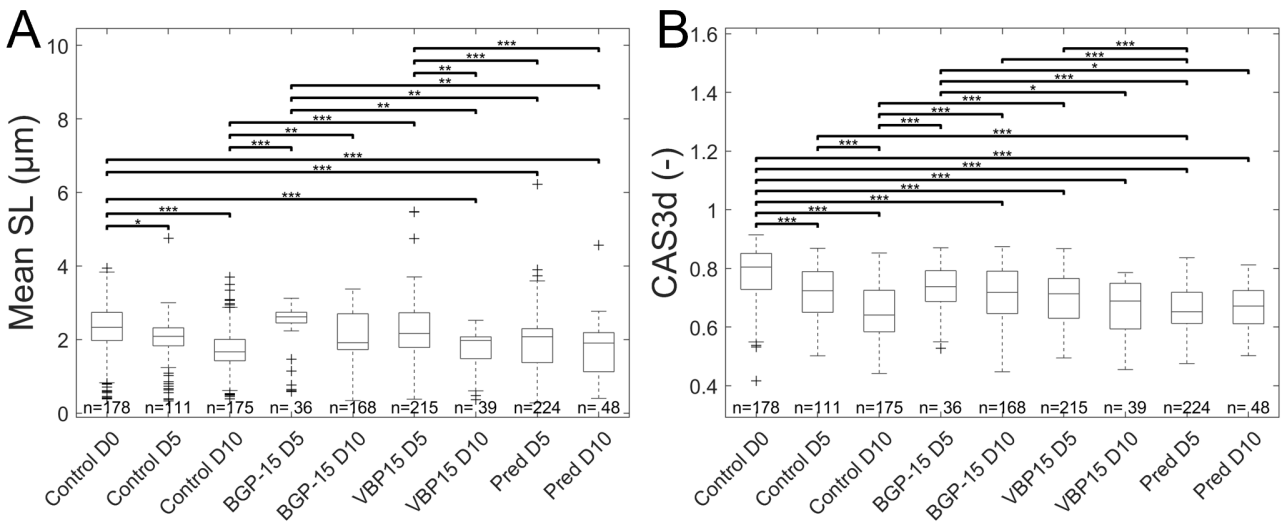


Fig. 8. **Evaluation of mouse diaphragm single muscle fibers in a ventilated animal model.** The animals were ventilated for 5 days (D5) and 10 days (D10). An unventilated group (D0) is included in the controls. The control group was untreated, apart from ventilation Four Treatment groups, three time points. The control groups show a significant decrease in both SL and CAS3d as compared to day 0